Measurements of microwave scattering by ultrasound in air at oblique incidence

Wingren, Niklas; Sjöberg, Daniel

Published in:
Europhysics Letters

DOI:
10.1209/0295-5075/131/54003

2020

Document Version:
Peer reviewed version (aka post-print)

Measurements of microwave scattering by ultrasound in air at oblique incidence

Niklas Wingren[1] and Daniel Sjöberg[1]

[1] *Department of Electrical and Information Technology, Lund University - Box 118, SE-221 00 Lund, Sweden*

PACS 41.20.Jb – Electromagnetic wave propagation; radiowave propagation
PACS 43.35.Sx – Acoustooptical effects, optoacoustics, acoustical visualization, acoustical microscopy, and acoustical holography

Abstract – Scattering of electromagnetic waves against acoustic waves has been studied in acousto-optics and radio acoustic sounding of the atmosphere, among others. Strong interaction requires phase matching, which occurs at two angles between waves. These depend on the wavelength ratio. The scattered electromagnetic wave is frequency shifted by the acoustic frequency, either up or down depending on the angle between waves. This work presents experimental verification of this scattering for 27.3 GHz microwaves and 40 kHz ultrasound in air. Both up- and down-shifting of the scattered wave is shown. Previous work has mostly focused on either nearly perpendicular or parallel incidence. In contrast, this work considers oblique incidence with frequencies differing from those used in acousto-optics and radio acoustic sounding.

Introduction. – Electromagnetic scattering by acoustic waves has been widely studied in the field of acousto-optics [1]. This started in the early 20th century with a prediction by Brillouin [2], resulting in experimental verification and deepening of the theory [1]. With the invention of the laser, acousto-optics grew and many devices were developed for manipulating laser beams [1]. As the name indicates, the electromagnetic frequencies in acousto-optics are in the optical range [3]. Ultrasound in the MHz range is often used in practical devices [4].

The interaction has also found use in meteorology through the Radio Acoustic Sounding System (RASS) [5]. This is a system measuring temperature and water vapor profiles in the atmosphere [6], and has been proposed for detecting aircraft wake vortices [7] as well as forest fires [8]. The system is often an addition to atmospheric radars for observation of clear air, with frequencies ranging from 10s of MHz to 1 GHz [6]. RASS requires an acoustic wavelength half that of the electromagnetic wavelength [5]. The relevant radar frequencies thus places acoustic frequencies in the audible range.

Though the frequency range for RASS differs from that in acousto-optics, the interaction mechanism is very similar. The basis of the interaction is the acoustic wave affecting dielectric properties of the medium [9]. It is commonly explained as the acoustic pressure modulating the density of the medium, which in turn modulates the refractive index [6]. This description is sufficient for fluid media, but a more complicated model is required for solid media [3].

In both acousto-optics and RASS, phase matching between the acoustic and electromagnetic waves is a crucial part of obtaining stronger scattering [3, 5]. This can only happen under very specific circumstances. For RASS and much of acousto-optics it is described by the Bragg condition, which relates the angle of incidence to the acoustic and electromagnetic wavelengths [9]. The condition is affected by parameters of the medium, which is how changing atmospheric conditions are detected in RASS [10]. In acousto-optics, devices such as modulators, scanners and filters utilize the Bragg condition to manipulate laser beams [3]. Another important detail is a frequency shift of scattered electromagnetic waves. For Bragg interaction, the shift is by a single acoustic frequency up or down [3, 9]. The frequency shift is not always used in acousto-optics, but it is crucial for RASS [9].

This work focuses on the Bragg mechanism, but other interaction mechanisms exist. Vibrations caused by acoustic excitation can be detected with radar as a Doppler-shifted echo, with possible applications in land mine detection [11] and non-destructive testing [12]. A similar mechanism uses amplitude modulated acoustic waves to cause vibration inside objects, which has been proposed for use in medical imaging [13]. Both of these interaction mechanisms can be explained using the micro-Doppler ef-

fect [14]. In the emerging field of ultrasound-mediated optical tomography, a frequency shift is instead caused in light from ultrasound modulation of optical path length and refractive index [15].

This work presents experimental verification on Bragg diffraction of electromagnetic waves by acoustic waves for a novel frequency range and incidence of the waves. The frequency of the electromagnetic waves was 27.3 GHz, placing them near the mm-wave range. The acoustic waves were 40 kHz ultrasound. For these frequencies in air, the angle between the wave vectors was determined (from the Bragg condition) to be 50°. This is between acousto-optics which has nearly perpendicular incidence and RASS which has parallel incidence. The emphasis of the measurements was to detect scattered power at the expected angle and frequency shift.

Interaction Mechanism. – The interaction mechanism of interest to this work has its basis in photoelasticity. In general, photoelasticity relates the displacement gradient in a medium to the inverse of the relative permittivity tensor [16]. The full formulation uses a fourth-rank photoelastic tensor with no symmetry, which is necessary for many solids [16]. In this work though, a much simpler scalar relation is assumed as is often done in acousto-optics [1,3]. For small perturbations in a mechanically and electrically isotropic medium where the photoelastic tensor has equal components, the following can be derived from a more complete tensor relation [17]

$$\varepsilon_1 = \frac{\varepsilon_r^2 \mathfrak{p}}{K} p. \tag{1}$$

Here, ε_1 is the perturbation in relative permittivity, ε_r is the unperturbed relative permittivity, $\mathfrak{p}$ is the scalar photoelastic constant, K is the bulk modulus and p is the pressure. The total permittivity is $\varepsilon = \varepsilon_0(\varepsilon_r + \varepsilon_1)$. Since an acoustic wave is a pressure variation, (1) shows that a permittivity variation can be expected to follow.

An electromagnetic wave incident on the acoustic wave is scattered against the dielectric perturbation, where stronger scattering can occur due to phase matching between the acoustic and electromagnetic waves [1, 3]. In acousto-optics, two types of scattering are commonly considered: Raman-Nath diffraction and Bragg diffraction [1]. What type is relevant depends on what is commonly called the Klein-Cook parameter [1, 18]

$$Q = \frac{2\pi\lambda L}{\Lambda^2} \tag{2}$$

where λ is the electromagnetic wavelength, L is the length for which the electromagnetic wave overlaps with the acoustic wave and Λ is the acoustic wavelength. Raman-Nath diffraction occurs for $Q \ll 1$ and Bragg diffraction for $Q \gg 1$ [18]. This work considers the case when $\lambda \sim \Lambda$ and the interaction length L is a number of wavelengths. Thus, Raman-Nath diffraction is not valid. For large L this work is clearly in the Bragg regime, but for L closer to Λ the interaction is still similar to Bragg diffraction [18].

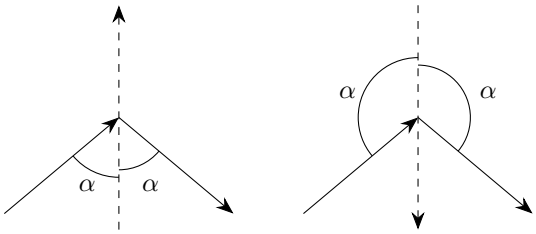

Figure 1: Propagation directions for acoustic (dashed) and electromagnetic waves where (3) holds. (−) case to the left and (+) case to the right.

In the Bragg regime, phase matching for given wavelengths λ and Λ can only occur for two orientations of the beams. This is described by the Bragg condition, which in acousto-optics is commonly defined using the angle of incidence [3]. However, in this work it is expressed equivalently as [17]

$$\cos\alpha = \mp\frac{\lambda}{2\Lambda} \tag{3}$$

where α is the angle between the acoustic and electromagnetic beams, λ is the electromagnetic wavelength and Λ is the acoustic wavelength. The scattered field has the same angle towards the acoustic wave as the incident field [3]. This is shown in fig. 1 for the two cases in (3).

One important property of the scattered field is that its frequency is shifted when compared with the incident field. This shift is $\pm F$ where F is the acoustic frequency [3]. The $\pm$ sign follows the same convention as the $\mp$ sign in (3). Thus, the frequency shift is positive if $\alpha > 90°$ and negative if $\alpha < 90°$. Further in this work (+) and (−) are used to denote scattering resulting in positive and negative frequency shifts.

Measurement Setup. – Measurements were performed in the microwave laboratory at Lund University, Sweden. A schematic view of the setup is shown in fig. 2. Two sets of measurements were performed: one where the ultrasound frequency was varied and one where the ultrasound wave was reflected.

Both the transmitting and receiving antennas were 26.5-50 GHz standard gain horns. The polarization of the antennas was perpendicular to the plane of interaction shown in fig. 2. The ultrasound source consisted of two 40 kHz transducers with their centers spaced roughly 1 cm and fed with the same signal. The geometry was set up for the (−) case of (3) such that $\alpha = 50°$ and $r = 22.5$ cm (see fig. 2). The antennas and ultrasound source are shown in fig. 3. Microwave absorbers where placed such that most of the direct microwave power would be either absorbed or reflected away from the receiving antenna.

The transmitted microwave signal was a 27.3 GHz continuous wave signal at a power of 20 dBm generated by an Agilent E8257D signal generator. The ultrasound signal

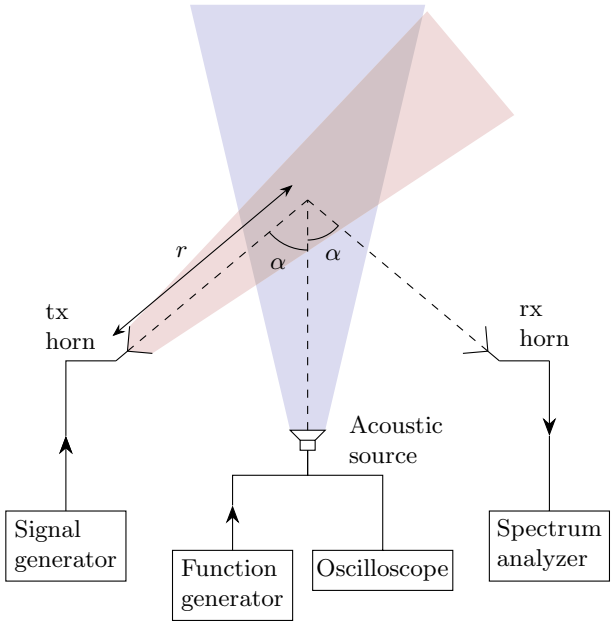

Figure 2: Setup and geometry for measurements.

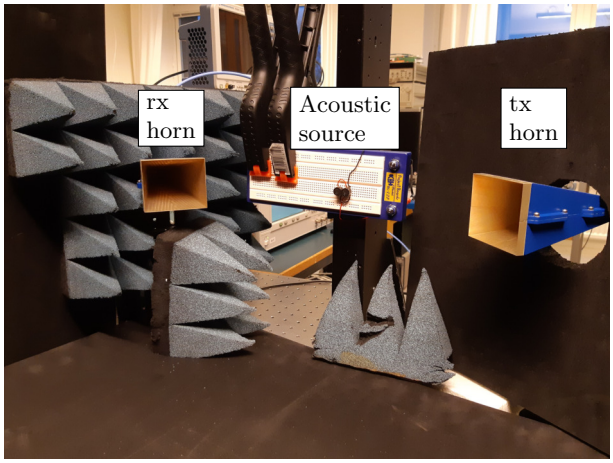

Figure 3: Antennas and ultrasound source.

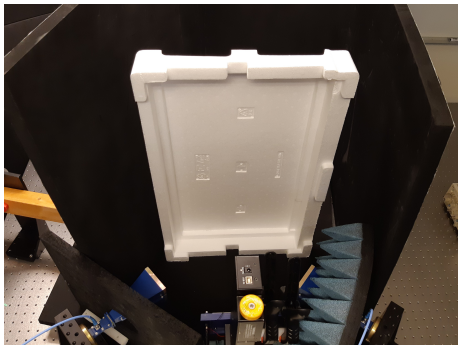

Figure 4: Setup with polystyrene sheet as ultrasound reflector.

was a 40 kHz modified square wave with a peak voltage around 15 V generated by a Tektronix FG504 function generator. The ultrasound signal was measured using a Rohde & Schwarz RTB2004 oscilloscope for inspection of the signal characteristics. The received microwave signal was measured using a Rohde & Schwarz FSU50 spectrum analyzer. For all measurements it had a resolution bandwidth set to 10 Hz and a video bandwidth set to 1 Hz. Logarithmic averaging was applied over 10 sweeps.

Equation (3) would suggest a microwave frequency of 27.43 GHz for maximum scattering, given $\alpha = 50°$ and an ultrasound frequency of 40 kHz. However, due to uncertainties in the angle the actual maximum would not necessarily be at that frequency. In addition, the system response varied with the microwave frequency. After varying the microwave frequency, 27.3 GHz was found to maximize the scattered microwave signal.

In the first set of measurements, the ultrasound frequency was varied to investigate the effect on the frequency shifted microwave signal. Due to instrument limitations such as phase noise, it was difficult to achieve good precision for the ultrasound frequency. Three different ultrasound frequencies on the order of 10 Hz away from 40 kHz were used. Measurements were taken in spans of 200 Hz around the transmitted microwave frequency and 40 kHz below.

In the second set of measurements, the ultrasound beam was reflected to investigate the (+) case of (3). For a beam reflected 180°, the new angle α results in (3) holding for the (+) case. To achieve a good ultrasound reflection without excessively affecting the microwave beam, a sheet of polystyrene was placed in front of the ultrasound source as shown in fig. 4. The sheet was placed such that it would not block the overlap of the ultrasound and microwave beams. The result of this should involve a standing ultrasound wave, but in this work it is more practical to view it as two beams with opposite propagation directions. Measurements were taken in spans of 200 Hz around the transmitted microwave frequency, 40 kHz above and 40 kHz below.

Results. – The waveform used for the ultrasound signal is shown in fig. 5. Variation of instrument parameters for maximum amplitude in combination with distortion from the ultrasonic transducers caused the unconventional waveform. The frequency was varied between measurements, which caused slight variation in the waveform. In general, no frequency shifted microwave signal was observed if the ultrasound source was turned off. With the ultrasound source turned on, a frequency shifted microwave signal could be observed. The frequency of this new microwave signal depended, as expected, on the microwave and ultrasound frequencies. When the microwave frequency was increased and approached 30 GHz, the power of the frequency shifted microwave signal decreased.

The results from the first set of measurements are shown in figs. 6 and 7. Figure 6 shows the leaked microwave signal directly transmitted between the two horns. The peak

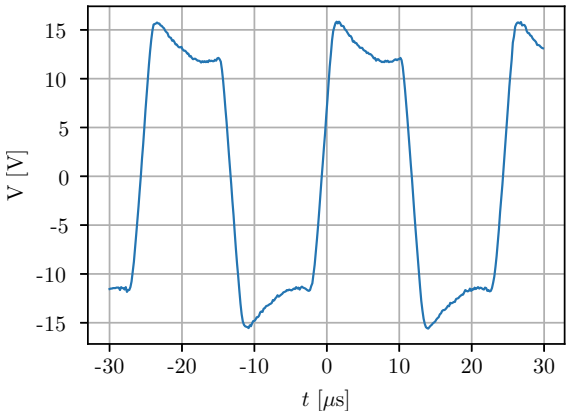

Figure 5: Ultrasound waveform used in measurements.

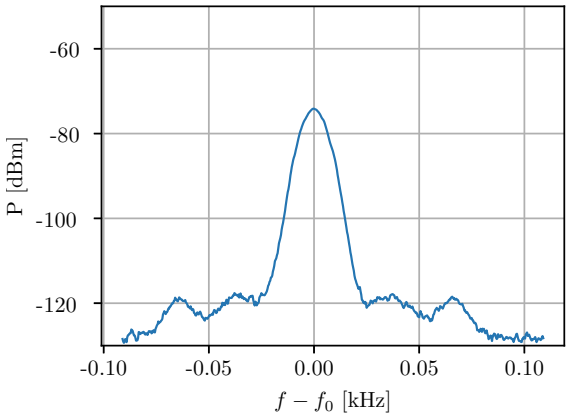

Figure 6: Microwave signal for direct transmission between horns. $f_0 = 27.300000275$ GHz.

power level of -74 dBm gives an isolation of 94 dB between the transmitter and receiver without acoustic power. This leaked signal was used to determine characteristics for the transmitted microwave signal. It can be seen that there are peaks at frequencies other than the center frequency. These were present regardless of the state of the ultrasound source, and are therefore assumed to be due to sidelobes in the signal generator. The center frequency in fig. 6 was measured to be 275 Hz above 27.3 GHz. This actual center frequency f_0 is also used when comparing the scattered microwave signals. The 3 dB linewidth in fig. 6 is 10 Hz and the 10 dB linewidth is 18 Hz. The frequency shifted microwave signals from the three ultrasound frequencies are shown in fig. 7. It can be seen that they are all within 100 Hz of $f_0 - 40$ kHz. Their frequency shifts are clearly different, which is to be expected since the ultrasound frequencies were different. The 3 dB linewidths of the peaks are (from left to right in fig. 7) 12 Hz, 11 Hz and 10 Hz while the 10 dB linewidths are 26 Hz, 21 Hz and 23 Hz. The linewidths of the frequency shifted microwave signals were thus on the same order of magnitude as that of the signal generator. The acoustic linewidth can also be expected to affect the linewidths in fig. 7, but this linewidth was not recorded.

The results from the second set of measurements are shown in figs. 8 and 9. The direct transmission microwave signal was similar to that in fig. 6 but with a level of the peak roughly 15 dB higher. This can be explained by reflection of the transmitted beam by the polystyrene sheet. The actual center frequency f_0 in this case was 162 Hz above 27.3 GHz. Figure 8 shows the microwave signal with a negative frequency shift. It is very similar in shape and power level compared with the signals in fig. 7, which is to be expected since the involved beams are mostly unaffected by the polystyrene reflector. Figure 9 shows the microwave signal with a positive frequency shift. This is roughly 10 dB weaker than previous scattered microwave signals, but it is still possible to distinguish it from the noise. For clarification, no such signal was present before the addition of the polystyrene sheet. The weakening

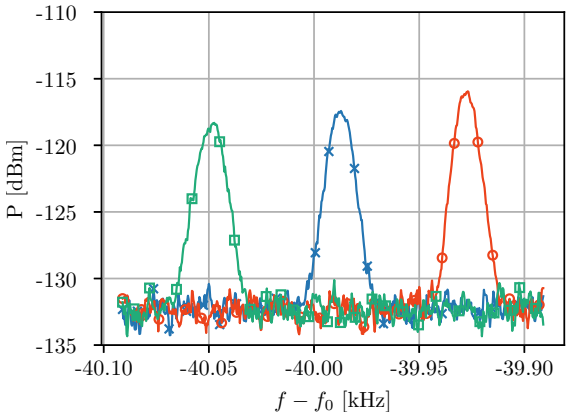

Figure 7: Frequency shifted microwave signals for different ultrasound frequencies. Frequency scale relative to $f_0 = 27.300000275$ GHz.

when compared with previous signals is due to the ultrasound beam being reflected by the polystyrene sheet. As such it traveled a longer distance than the original beam, leading to a lower acoustic pressure and a lower scattered power. The peaks in fig. 8 and fig. 9 are both located at frequencies near 40 kHz from the transmitted frequency. However, the negative shift is 39.96 kHz while the positive shift is 39.93 kHz. The difference of 30 Hz can probably be attributed to oscillator drift, especially since the two measurements were not taken simultaneously.

Discussion. – Measurements verified that the scattering as predicted by (3) occurred with the expected frequency shifts and with the expected angle α. A significant change in the wavelength ratio with α fixed resulted in a decrease in received power. This showed that if (3) does not hold, the scattered power is affected. The results are in accordance with established research fields and technologies relying on this type of scattering.

However, most measurements known to the authors have used other ratios between λ and Λ. The most established field investigating this kind of interaction is acousto-

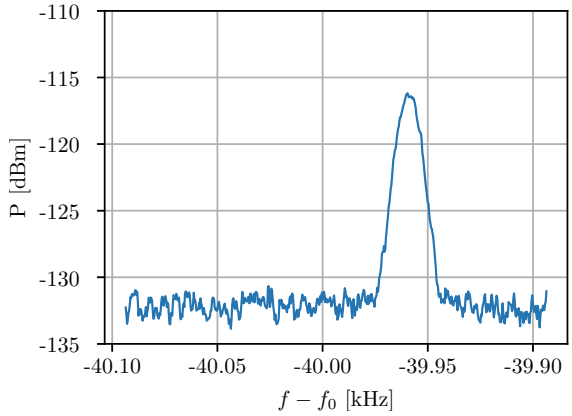

Figure 8: Microwave signal for negative frequency shift. Frequency scale relative to $f_0 = 27.300000162$ GHz.

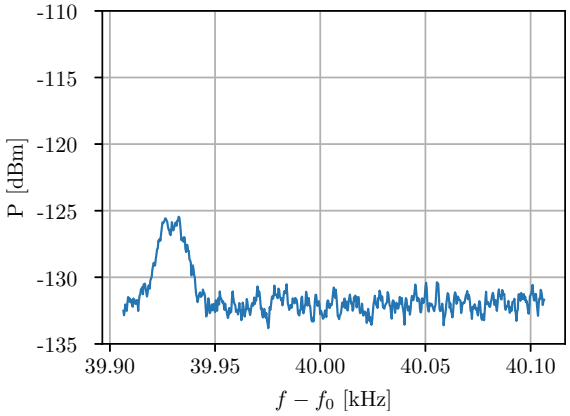

Figure 9: Microwave signal for positive frequency shift. Frequency scale relative to $f_0 = 27.300000162$ GHz.

optics where commonly $\lambda \ll \Lambda$ [3]. The incidence of beams in acousto-optics is close to perpendicular, both in the Raman-Nath and Bragg regimes [3]. In RASS, the system is set up with collocated transmitters and receivers such that the scattered wave is focused back at the receiver [5]. The incidence is then parallel, necessitating $\lambda = 2\Lambda$. The current work has a ratio λ/Λ which is closer to that of RASS than that of acousto-optics.

Nevertheless, there are some significant differences between parallel and oblique incidence. The aforementioned focusing back towards the receiver should provide a possibility of increased scattered power [5]. Furthermore, with parallel incidence the overlap between the acoustic and electromagnetic beams is theoretically infinite, although in practice it depends on the length of pulsed signals [9]. For oblique incidence, the overlap is determined by the beamwidths and the angle α.

To increase the scattered electromagnetic power, a fairly obvious action would be to increase the power emitted by the acoustic source. This would result in a higher acoustic pressure and subsequently, as can be seen from (1), a higher dielectric perturbation. Another improvement would be to use larger arrays for both the acoustic and electromagnetic sources. This can be understood from the plane-wave spectrum of the sources. An arbitrary single-frequency wave can be seen as a spectrum of plane waves with different wave vectors, where power is divided among the modes [19]. In this work, α is the angle between the acoustic and electromagnetic wave vectors $\boldsymbol{q}$ and $\boldsymbol{k}$. For a given α, phase matching is only obtained for $\boldsymbol{q}$ and $\boldsymbol{k}$ fulfilling the Bragg condition. Due to tolerance in the Bragg condition, wave vectors close to these also contribute to the received power [3]. Parts of the plane-wave spectra far from the optimal $\boldsymbol{q}$ and $\boldsymbol{k}$ contribute less. Using larger arrays, power can be concentrated to parts of the plane-wave spectra near the optimal $\boldsymbol{q}$ and $\boldsymbol{k}$ which should increase the received power.

The interaction between ultrasound and microwaves presented in this work has a potential application in non-destructive testing with a length scale of interest near 1 cm. A contrast in effective material properties, as caused by a defect, affects the Bragg condition and in turn the amplitude of the frequency shifted signal. This is similar to how RASS works [10]. Microwaves and ultrasound are used individually in non-destructive testing, but a combined system would be sensitive to contrasts in both electromagnetic and acoustic properties of a sample. This could lead to better detection of low-contrast defects, which has been stated as an advantage for combining ultrasound and microwaves in medical imaging [13]. Some examples where microwave and ultrasonic testing are used individually at length scales near 1 cm are timber [20,21], concrete structures [22,23] and thick composites [24]. Another possible application is detection of uneven ultrasonic propagation. Effects such as reflections and wave guiding can cause ultrasonic propagation in undesired directions when performing ultrasonic non-destructive testing. The interaction with an incident microwave would be altered by these effects, possibly allowing for detection using the frequency shifted microwave signal. The weak interaction strength observed during measurements might be an issue for practical applications. However, measurements in this work were performed in air where interaction is expected to be very weak due to its photoelastic constant $\mathfrak{p} = 0.00059$ [25]. Other media can have $\mathfrak{p}$ several orders of magnitude higher than this [26,27].

Conclusions. – The scattering of microwaves against ultrasound in air was measured. The effects of Bragg diffraction could be observed. An electromagnetic wave incident on an acoustic wave at the Bragg angle was scattered with a negative frequency shift corresponding to the ultrasound frequency. A slight change of the acoustic frequency resulted in a corresponding change in the frequency shift. A large change in the microwave frequency reduced scattered power at the original angle.

Reflection of the acoustic wave gave rise to a new scattering component with a positive frequency shift corresponding to the acoustic frequency. Thus, for given acous-

tic and electromagnetic frequencies both up- and down-shifting Bragg diffraction was observed.

* * *

The authors would like to thank J. Nilsson from the Department of Biomedical Engineering, Lund University for valuable discussions and for providing the ultrasonic transducers used in the measurements. This work was supported in part by the Swedish Armed Forces, in part by the Swedish Defence Materiel Administration, in part by the National Aeronautics Research Program and in part by the Swedish Governmental Agency for Innovation Systems.

References

[1] Korpel A., *Acousto-optics* 1st Edition Optical engineering, 16 (Marcel Dekker Inc, New York) 1988.
[2] Brillouin L., *Ann. Phys.*, **9** (1922) 88.
[3] Saleh B. E. A. and Teich M. C., *Acousto-Optics* 2nd Edition Fundamentals of Photonics (John Wiley & Sons, Inc., Hoboken, New Jersey) 2007 Ch. 19 pp. 804–833.
[4] Savage N., *Nat. photonics*, **4** (2010) 728.
[5] Marshall J. M., Peterson A. M. and Barnes A. A., *Appl. Opt.*, **11** (1972) 108.
[6] Fukao S. and Hamazu K., *Radar for Meteorological and Atmospheric Observations* (Springer Japan) 2014.
[7] Rubin W. L., *J. atmos. ocean. technol.*, **17** (2000) 1058.
[8] Sahin Y. G. and Ince T., *Sensors (Basel)*, **9** (2009) 1485.
[9] Gurvich A. S., Kon A. I. and Tatarskii V. I., *Radiophys. quantum electron.*, **30** (1987) 347.
[10] May P. T., Strauch R. G., Moran K. P. and Ecklund W. L., *IEEE trans. geosci. remote sens.*, **28** (1990) 19.
[11] Scott W. R. and Martin J. S., *Proc. SPIE*, **3710** (1999) 204 .
[12] Buerkle A. and Sarabandi K., *IEEE trans. antennas propag.*, **57** (2009) 3628.
[13] Tafreshi A. K., Top C. B. and Gençer N. G., *Phys. med. biol.*, **62** (2017) 4852.
[14] Chen V. C., Li F., Ho S. . and Wechsler H., *IEEE trans. aerosp. electron. syst.*, **42** (2006) 2.
[15] Elson D. S., Li R., Dunsby C., Eckersley R. and Tang M.-X., *Interface Focus*, **1** (2011) 632.
[16] Nelson D. F. and Lax M., *Phys. rev. B*, **3** (1971) 2778.
[17] Wingren N., *Acousto-electromagnetic interaction in materials for aerospace composites* M.s. thesis Dept. of Elect. and Inform. Technol., Lund Univ., Lund, Sweden (2019).
[18] Klein W. R. and Cook B. D., *IEEE trans. sonics ultrason.*, **14** (1967) 123.
[19] Orfanidis S. J., *Diffraction – Plane-Wave Spectrum* Electromagnetic Waves and Antennas (Rutgers University) 2016 Ch. 19 pp. 844 – 922.
[20] Riggio M., Sandak J. and Franke S., *Constr. build. mater.*, **101** (2015) 1241 .
[21] Vössing K. J. and Niederleithinger E., *Holzforschung*, **72** (2018) 467 .
[22] McCann D. and Forde M., *NDT & E International*, **34** (2001) 71 .
[23] Rehman S. K. U., Ibrahim Z., Memon S. A. and Jameel M., *Construction and Building Materials*, **107** (2016) 58 .
[24] Ibrahim M., *Compos., Part A Appl. sci. manuf.*, **64** (2014) 36 .
[25] Wingren N. and Sjöberg D., *Analytical modeling and multiphysics simulation of acousto-electromagnetic interaction* in proc. of *2020 14th European Conference on Antennas and Propagation (EuCAP)* 2020 pp. 1–5.
[26] Dixon R. W., *J. appl. physi.*, **38** (1967) 5149.
[27] Uchida N., *Japanese Journal of Applied Physics*, **7** (1968) 1259.